

# Mechanics Analyses of Boxer's Fracture

Alex J. McMullen<sup>1</sup>, Ahmed Abdel-Mohti<sup>2</sup>, Saad A. Almagahwi<sup>1</sup>, Makenzie Loudon<sup>1</sup>, Bryan D. Recker<sup>1</sup>, Hui Shen<sup>1\*</sup>

<sup>1</sup>*Department of Mechanical Engineering, Ohio Northern University, Ada, OH 45810, USA*

<sup>2</sup>*Department of Civil Engineering, Ohio Northern University, Ada, OH 45810, USA*

\* *Corresponding Author: Hui Shen, h-shen@onu.edu*

**Abstract:** Boxer's fracture is one of the most common sports injuries. It localizes specifically in some positions of the fifth metacarpal bone of the hand. Experimental and analytical studies have been carried out in this project in order to investigate the issue thoroughly. In the experiment phase, a typical fifth metacarpal bone has been tested using a test setup that includes the proper constraints and loads with different orientations. Three-dimensional finite element modeling of the fifth metacarpal bone in the context of the whole hand has been performed to determine the causes of such fracture. In light of results of the experimental and numerical studies, potential reasons that may contribute to the boxer's fracture will be provided. The outcomes of this work may not only help to avoid this kind of fracture, but also assist surgeons to find more effective ways of treatments.

Key words: biomechanics, boxer's fracture, finite element analysis

## 1 Introduction

Boxer's fracture is a common name for a fracture of the fifth metacarpal bone of the hand. The fracture localizes specifically in some positions of the fifth metacarpal bone, and results from a compression force acting on a flexed metacarpophalangeal joint [1] – usually when a closed fist strikes a firm or immovable object with force or the bone is hit by a flying object. Due to the nature of the injury, it is a common fracture suffered by athletes.

Although the boxer's fracture is one of the most common hand injuries, accounting for 20% of all hand fractures [2], there is still a lot of debate in terms of the treatment and prevention of the injury. Treatment for a fracture of the fifth metacarpal varies from non-operative procedures, such as different forms of cast immobilization [1] or full dynamic treatment [3], to surgical techniques, such as internal fixation with the use of screws and K-wire pinning [4]. To prevent the fracture from healing in malrotation or in volar angulation, surgical treatment is always indicated when the fracture is severely displaced and unstable, as the severe condition may cause loss of hand function [4]. However, the terms 'severely displaced' and 'unstable' are up for interpretation, as some proponents of non-operative full mobilization treatment hypothesize that the fracture will heal properly without surgery as long as the volar angulation does not exceed 70° [3]. In accordance with Ali et al [5], no clinical study has yielded a conclusive answer as to how much angulation of a boxer's fracture is acceptable.

The acceptable treatment, prevention, and angulation of the fracture is further complicated due to the fact that the boxer's fracture has been found to localize in various locations in the fifth

metacarpal. Most technical literature defines the boxer's fracture as a fracture in the neck of the bone [1]. However, a study conducted in 2010 provided evidence that fractures of the fifth metacarpal caused by punching-type injuries also commonly occurred at locations aside from the neck - namely at the shaft and the base of the bone [6]. Therefore, a clear understanding of force orientation and location versus boxer's fracture location has not been clearly identified.

The objective of this study was to gain a better understanding of the mechanics of the boxer's fracture, in particular the location of the fracture due to different directions of applied force. To perform this mechanical analysis, fifth metacarpal samples were tested using a test setup that includes the proper constraints and loads at orientations of 0°, 30°, 60°, and 90° from the longitudinal axis of the bone. 3-Dimensional finite element analyses (FEA) were performed to simulate the boxer's fracture. The results from experiments and simulations were compared in terms of load direction versus fracture location. The results obtained from this mechanical analysis is expected to provide useful insight as to how the geometry of the fifth metacarpal bone influences the location at which the bone will fracture when subjected to different loading conditions. The results of this study can be combined with clinical observations to gain a better understanding of the boxer's fracture. This investigation would also provide suggestions on how to prevent the boxer's fracture in various positions.

## **2 Sample Preparation and Materials**

Polymer models of the fifth metacarpal bone were used for experimental testing. The test samples were made of poly lactic acid (PLA), which is a brittle thermoplastic commonly used for additive manufacturing. To accurately model the geometry of a fifth metacarpal, an actual fifth metacarpal bone was scanned using a MakerBot Digitizer desktop 3D scanner. The scanned 3D model data was then imported into SolidWorks 3D modeling software, where the surface was smoothed out and the model was measured to ensure accuracy. The model was then converted to STL file format, so that it could be extruded using a 3D printer. In the MakerWare software, the infill was set to 10% and the layer height was set to 0.20 mm so that when printed, the middle of the shaft would be less dense than the shell - as the case in real bone.

Although using real bone samples would have been ideal, PLA models were chosen primarily because of availability. To refine the testing methods and run an ample number of tests, numerous bone samples were needed. A dozen PLA samples could be created in a matter of hours with the 3D printer. The purpose of the current work is to study the force orientation and location versus boxer's fracture location, so PLA models would yield the necessary results for this experiment. As long as the PLA models were accurate in terms of geometry, the samples should fail in the same location. However, it should be noted herein that, polymers do not demonstrate the same mechanical behavior as bone – plastic is relatively ductile and bone is brittle.

## **3 Experimental Procedures**

To simulate the boxer's fracture, PLA fifth metacarpal samples were secured in fixtures and subjected to static compression until failure. Samples were oriented at different angles to observe the effects of direction and location of compressive force on the location of failure in the

sample. A custom clamp fixture was designed and built for the Instron compression system to hold the irregular shaped bone samples in place at each orientation (except for 90°). The 3D model of the custom clamp can be seen in Figure 1. Small screws were used to hold the head and base of the bone in place during compression. Small foam pads were stuck to the top surface of the head fixture and the bottom surface of the base fixture to ensure that the bone did not slide on the metal surface.

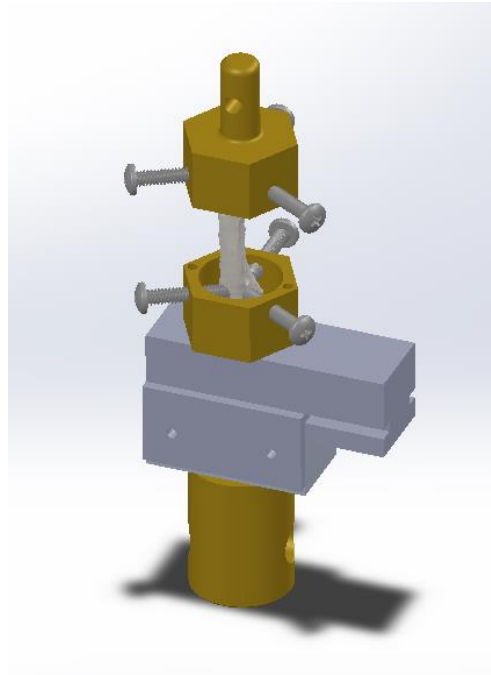


Figure 1: 3D model of the custom clamp fixture used for experimental testing.

The first round of compression testing was performed when the samples were oriented at 0°. This was when an axial load was applied to the sample, or in other words when the longitudinal axis of the sample was parallel to the compressive force. This orientation can be seen in Figure 2a. Five samples were compressed until failure. Data of the displacement and load was collected using Instron software. The procedure was repeated five times for each orientation. Orientations at angles of 30° and 60° were also tested. The setup of the 30° and 60° orientations can be seen in Figure 2b and Figure 2c, respectively.

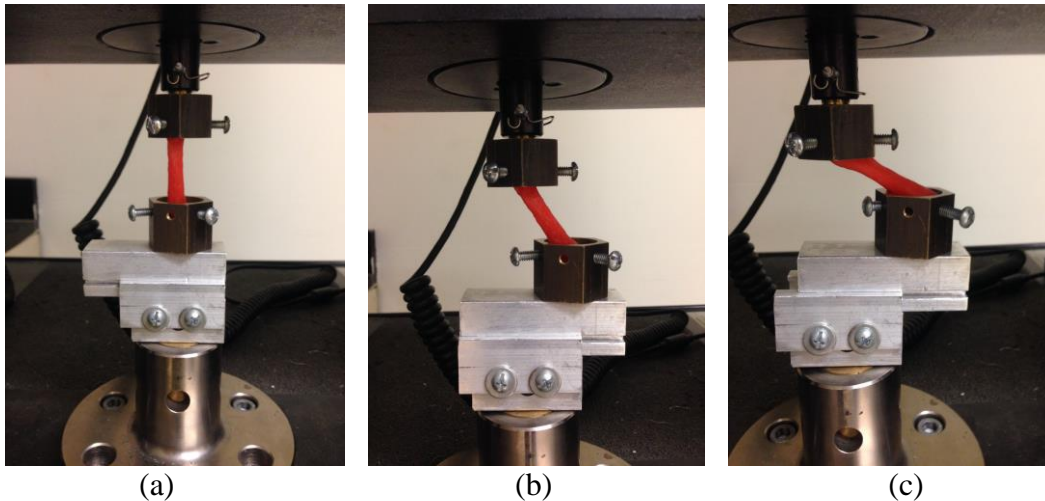


Figure 2: Compression test setups at orientations of (a)  $0^\circ$ , (b)  $30^\circ$ , and (c)  $60^\circ$ .

The last orientation was an angle of  $90^\circ$ , or when the longitudinal axis of the bone sample was perpendicular to the load. For this orientation, the samples were placed on a three-point flexure fixture. Two lower anvils acted as simple supports at the head and base of the bone samples. The upper anvil applied the load on the shaft of the sample. This orientation can be seen in Figure 3. For this orientation, five samples were tested when the upper anvil applied a force at a distance between the center of the shaft and the head (approximately 2.5 cm from the head), which is referred to as Force 1 in this paper. Other samples were tested when the upper anvil applied a force at a distance between the center of the shaft and the base (approximately 2.5 cm from the base), which is denoted as Force 2 in this paper. This method was used to observe if the location of the fracture was dependent on the lateral location of the applied force. The data was not collected for these samples, but pictures were taken for visual comparison.

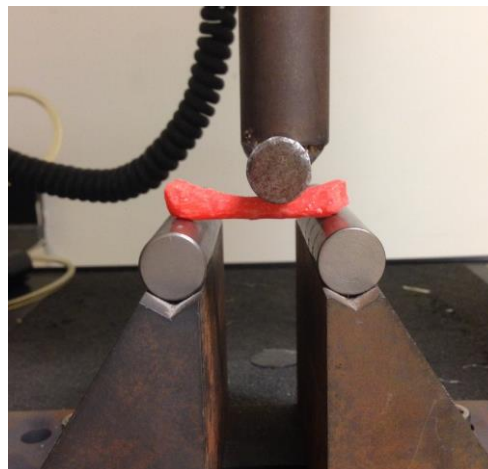


Figure 3: Compression test setup at  $90^\circ$  orientation.

## 4 Finite Element Analysis

A 3D finite element analysis (FEA) was performed on the 3D model of the fifth metacarpal bone using ANSYS software. The material properties used for the fifth metacarpal bone in the FE analysis are shown in Table 1. The properties specified are mechanical properties of human cortical bone based on data from Reilly and Burstein, Journal of Biomechanics, 8 (1975) [6]. While bone consists of cortical and trabecular bone, using cortical bone best represented the neck and shaft of the bone. Cortical bone also has less variation in mechanical properties than trabecular bone, as trabecular bone strongly depends on factors that vary based on anatomic site, age, and disease [7]. Again, it should be mentioned that this investigation focuses on the location of failure in relation to the geometry, so the accuracy of the material properties is not critical.

Table 1: Fifth metacarpal material properties used for FEA model.

Property	Value	Unit
Isotropic Elasticity		
Derive from	Young's Modulus	
Young's Modulus	17.0	GPa
Poisson's Ratio	0.45	
Bulk Modulus	28.3	GPa
Shear Modulus	6.07	GPa

Just as in the experimental procedure, forces were applied to the bone at angles of 0°, 30°, 60°, and 90° from the longitudinal axis. For angles of 0°, 30°, and 60°, the base of the bone was fixed and a compressive force was applied on the head of the bone at the desired magnitude and direction. The magnitude assigned to each force was equal to the average maximum force obtained in the corresponding experimental test. Those magnitudes will be specified in the results section in Table 2. The z-axis in the FE model was considered to be the longitudinal direction for the FEA. It should be noted that the z-axis is not the exact longitudinal axis of the bone, due to the bone's odd shape and the method in which the bone was modeled in SolidWorks. Therefore, it can be seen that the 0° force is not an exact axial load (Figure 4). However, it was ensured that this coordinate system remained consistent throughout the entirety of the FEA testing. The constraints and applied forces for the 0°, 30°, and 60° orientations can be seen in Figure 4, 5, and 6, respectively. To reiterate, the magnitudes given to each applied force are specified in the results section, so notice that the magnitudes of the forces as shown in Figure 4-6 are merely set to a default value of 500 N, which is just used to show the orientation of each force.

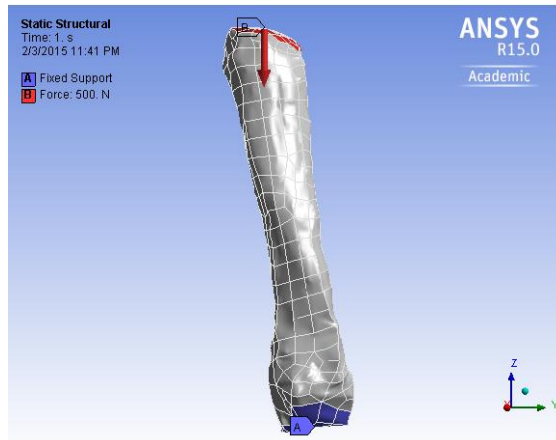


Figure 4: FEA constraints and applied forces for 0° orientation.

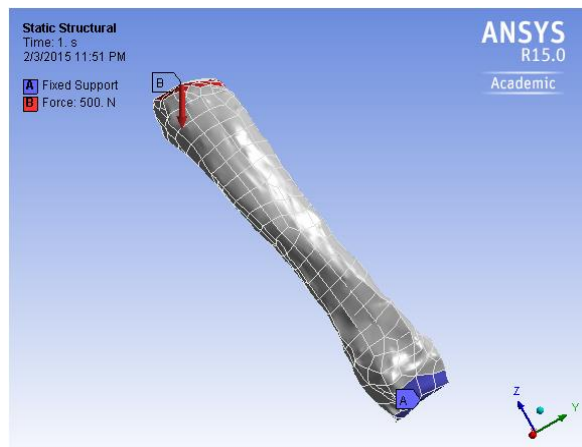


Figure 5: FEA constraints and applied forces for 30° orientation.

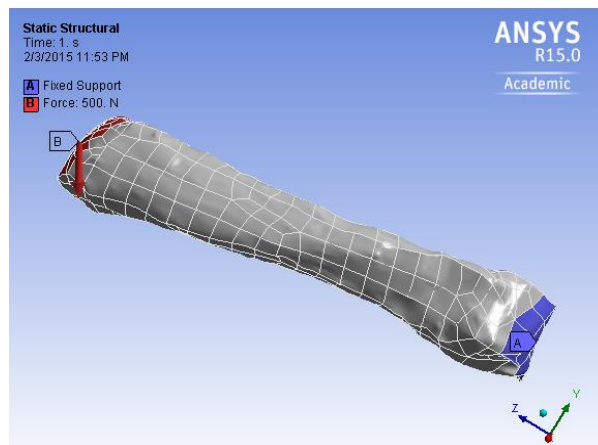


Figure 6: FEA constraints and applied forces for 60° orientation.

For the simulation of the 90° orientation, faces of the head and base perpendicular to the longitudinal axis were fixed. A force was applied perpendicularly to the longitudinal axis (in the y-direction) at a point along the shaft of the bone on the side opposite the fixed constraints. Just as in the experimental procedure, two simulations were run, with one force applied closer to the

head of the bone (Force 1), and another force applied closer to the base of the bone (Force 2). Note that the placement of these forces was intended to simulate a force on the lateral (outside) face of the fifth metacarpal bone. Like the other orientations, the magnitude assigned to each force at  $90^\circ$  was equal to the average maximum force obtained in the corresponding experimental test. The y-axis in the FE model was considered to be perpendicular to the longitudinal axis of the bone. Much like the inaccuracy of the z-axis as previously explained, the y-axis is not exactly perpendicular to the longitudinal axis of the bone. The constraints and applied forces for the  $90^\circ$  orientation with Force 1 and the  $90^\circ$  orientation with Force 2 can be seen in Figures 7 and 8, respectively. Once again, the magnitudes given to each applied force are specified in the results section, so notice that the magnitudes of the forces as shown in Figure 7 and 8 are also set to a default value of 500 N.

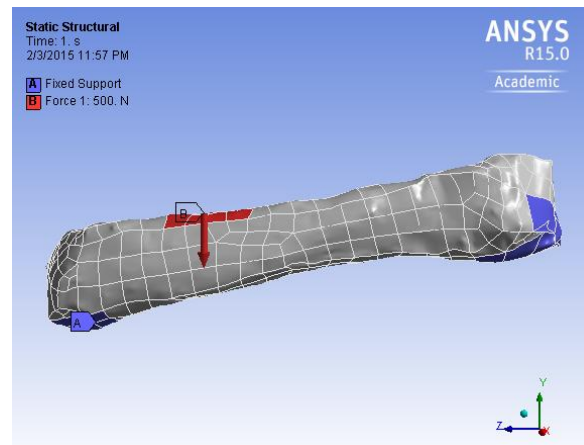


Figure 7: FEA constraints and applied forces for  $90^\circ$  orientation; Force 1.

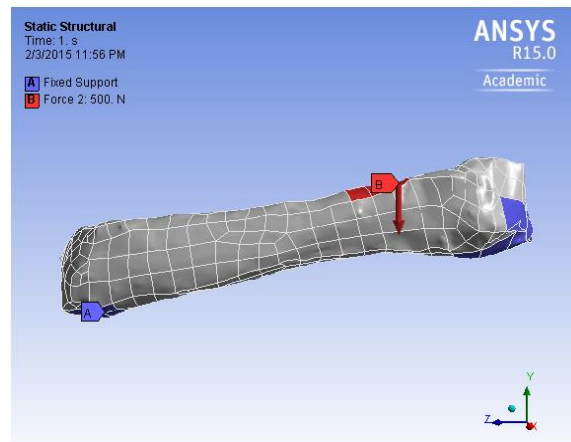


Figure 8: FEA constraints and applied forces for  $90^\circ$  orientation; Force 2.

Plots of the equivalent von Mises stresses for each orientation were obtained using ANSYS software. These plots were used for visual analysis and comparison with the experimental results.

## 5 Results and Discussion

### 5.1 Experimental Results

Table 2 shows the average maximum loads obtained for compression tests conducted at orientations of 0°, 30°, 60°, and 90°. Five compression tests were performed for each orientation, and data was obtained from each test. Note that at the 90° orientation, data was only collected for the five tests with Force 1. The results revealed an inverse relationship between the sample orientation angle and the maximum load. In other words, the average maximum load was found to decrease as the angle from the longitudinal axis increased. On average, the samples were over twice as strong in compression (0°) than in shear (90°).

Table 2: Average maximum load values for each orientation of experimental compression testing.

Orientation	Average Maximum Load (N)
0°	5.54E+02
30°	5.48E+02
60°	4.56E+02
90°	2.58E+02

For each compression test, a picture was taken of the sample after failure. The samples from each orientation were visually inspected to identify the general location of failure. Note that the two samples oriented at 90° with Force 2 were also visually inspected. Rather than taking measurements of the exact location of the failures in terms of distance, it was instead recorded as occurring in a general location of the bone, as well as identifying the general area that it favors, or is closest to (e.g. shaft, favoring the base). If the failure occurred in the base or head of the bone, it was simply recorded as failing at the base or the head. Table 3 shows the results of the visual inspection for each orientation of the experimental compression testing. The far right column of Table 3 refers to a figure of the sample with the most significant failure from each test, which can be seen below in Figures 9-13. Images of all of the samples for each orientation can be seen in the Appendix.

Table 3: Visual inspection results for each orientation of experimental compression testing.

Orientation	Location of Failure	Image of Sample
0°	Shaft, center	Figure 9
30°	Shaft, favoring the base	Figure 10
60°	Shaft, favoring the head	Figure 11
90° <sup>a</sup>	Shaft, favoring the head	Figure 12
90° <sup>b</sup>	Shaft, favoring the base	Figure 13

*a* – force applied closer to the head (Force 1),

*b* – force applied closer to the base (Force 2)



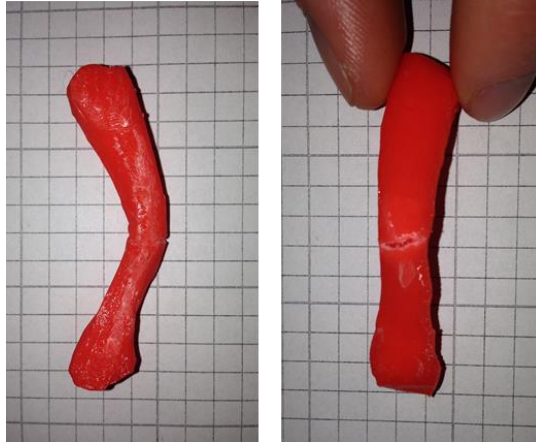


Figure 9: Sample with most significant failure at  $0^\circ$  orientation.

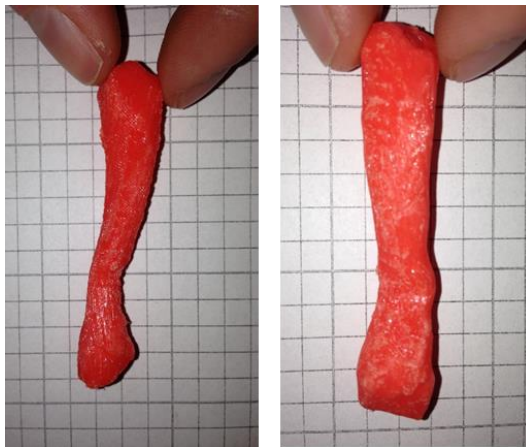


Figure 10: Sample with most significant failure at  $30^\circ$  orientation.

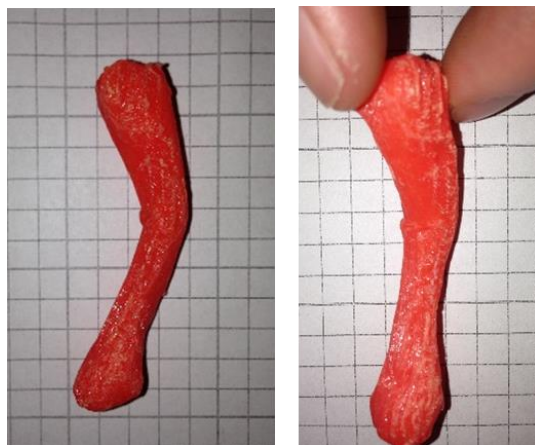


Figure 11: Sample with most significant failure at  $60^\circ$  orientation.

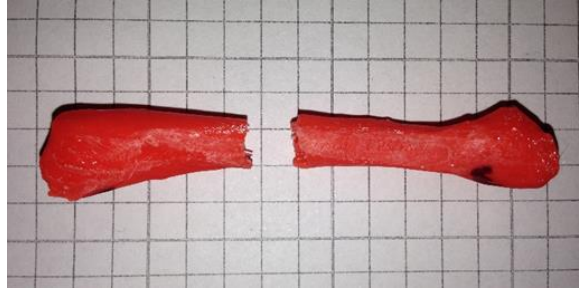


Figure 12: Sample with most significant failure at 90° orientation; Force 1.

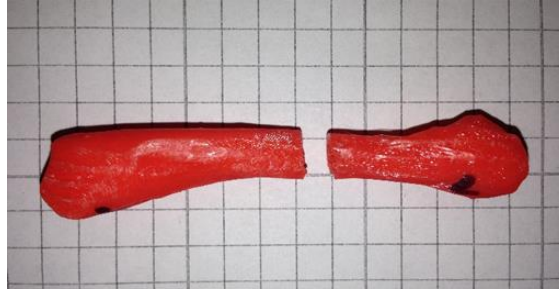


Figure 13: Sample with most significant failure at 90° orientation; Force 2.

The images in Figures 9-13 and the Appendix show that only the samples oriented at 90° completely fractured at the maximum load. All but one sample at 0° cracked without fracturing completely. Samples at 30° and 60° showed permanent deformation with no sign of external cracks. These results occurred due to the fact that the samples were plastic. Although PLA is considered to be relatively brittle, it is still not as brittle as bone.

## 5.2 FEA Results

Figures 14-18 show the equivalent von Mises stress results obtained from the finite element analysis performed using ANSYS software. The FEA results were obtained as a means of visual comparison to the experimental results. The force applied to each orientation corresponded to the average maximum load at each orientation of the experimental testing, which are listed in Table 2. Note that a force of 258 N was used for Force 1 and Force 2 for the 90° orientation.

When comparing the FEA results at 0° (Figure 14) with the experimental results at 0° (Table 3 and Figure 9), each showed that the bone was likely to fail close to the center of the shaft. Similarities can also be seen in both tests at an orientation of 30°. Referring to the FEA results in Figure 15, it can be observed that the bone will fail in the shaft, favoring the base. This is also true of the experimental results at 30° as seen in Table 3 and Figure 10. The FEA results for the 60° orientation did not support the experimental results for the 60° orientation. Figure 16 shows that the bone will fail in the shaft, favoring the base, when subjected to a force at 60°, as opposed to Table 3 and Figure 11, which show that the bone will fail in the shaft, favoring the head, when subjected to a force at 60°.

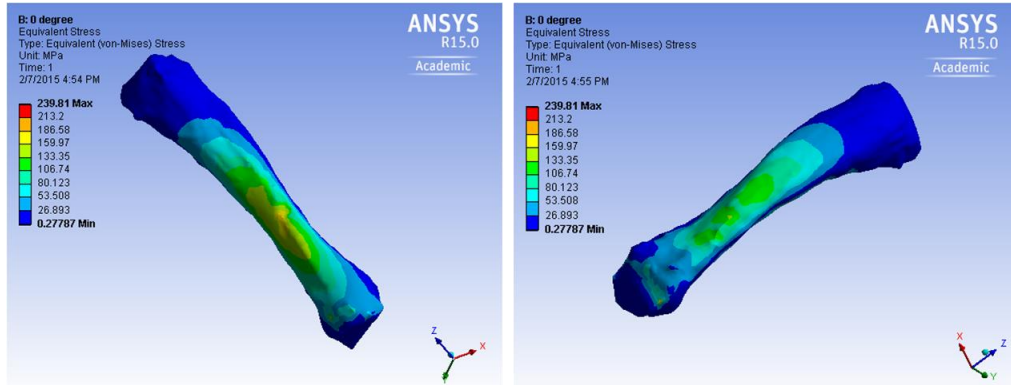


Figure 14: FEA von Mises results for 0° orientation.

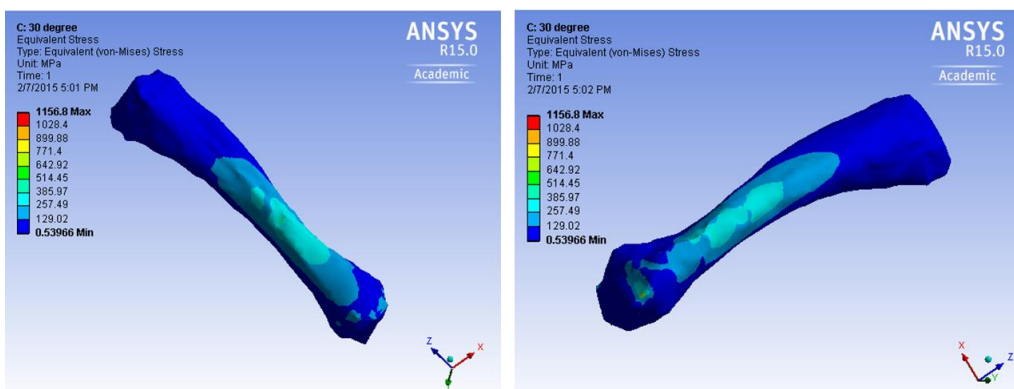


Figure 15: FEA von Mises results for 30° orientation.

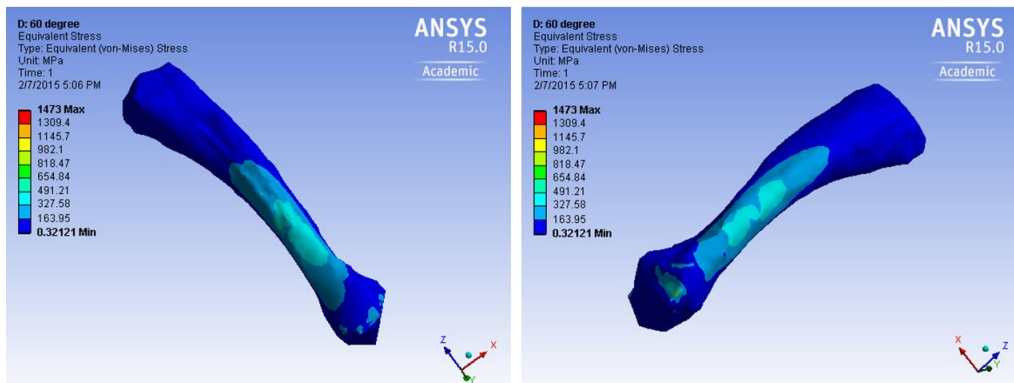


Figure 16: FEA von Mises results for 60° orientation.

The results for each test method are also similar for both cases of the 90° orientation. The FEA results for 90° orientation with Force 1 (Figure 17), and the corresponding experimental results (Table 3 and Figure 12), each demonstrated that the bone will fail closest to the head; which is also the location that Force 1 was applied. The FEA results for 90° orientation with Force 2 (Figure 18), and the corresponding experimental results (Table 3 and Figure 13), each demonstrated that the bone will fail closest to the base; which is also the location that Force 2 was applied.

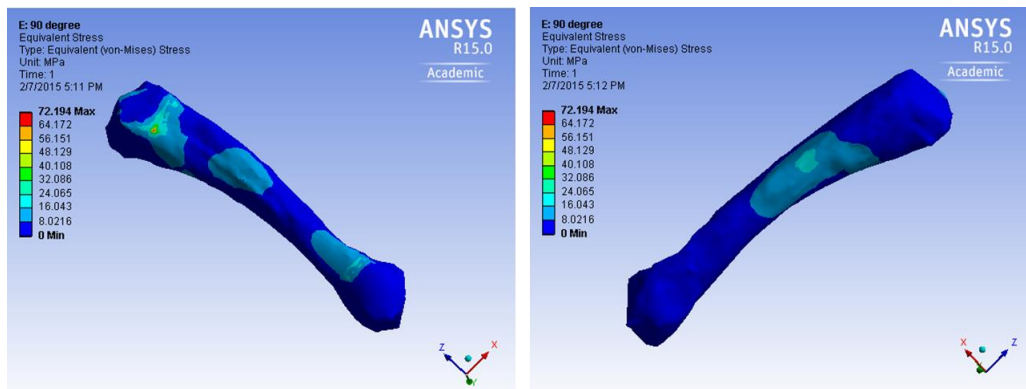


Figure 17: FEA von Mises results for 90° orientation; force applied closer to the head of the bone (Force 1).

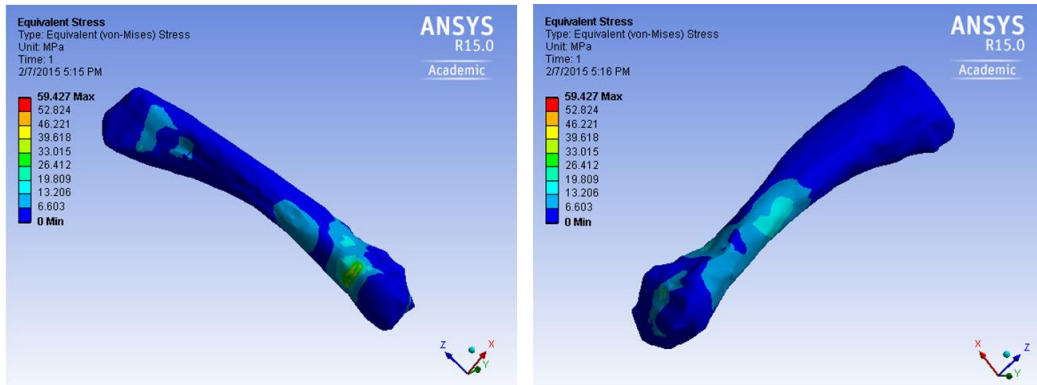


Figure 18: FEA von Mises results for 90° orientation; force applied closer to the base of the bone (Force 2).

Note that the maximum von Mises stress obtained for each analysis was shown close to the fixed support(s). This is most likely due to singularity caused by the fixed supports, and can therefore be ignored. This also means that results showing significant stress at the base of the bone cannot be considered accurate evidence of base fractures.

### 5.3 Discussion

First, the following is a summary of the overall results obtained from this investigation:

- The bone is strongest in pure compression (0°), and weakest in pure shear (90°).
- The bone is most likely to fail at the shaft, due to the bone geometry.
- When the bone is subjected to an axial load, it will most likely fail at a distance between the center of the shaft and the base of the bone.
- When a force is applied to the side of the bone, the bone will fracture at the location of the applied force.

Bone is designed to be strongest in compression, as this optimizes the bone for typical loading conditions, as the bone is usually loaded along its longitudinal axis [7]. Therefore, the experimental results shown in Table 2 are as expected. Much of the axial strength is said to

come from the cortical bone, but this study also shows that the geometry of the bone is also responsible for optimizing the bone in compression.

Many sources consider the boxer's fracture as a fracture that most commonly localizes in the neck of the fifth metacarpal, and results from a punching-type injury [1] – or in other words, when the bone is subjected to compressive forces. However, our investigation yielded that the fifth metacarpal bone is most likely to fracture in the shaft, closer to the base than the head, when subjected to a compressive force. In terms of geometry, the results of this study make the most sense from a mechanical perspective, due to the fact that the bone shows necking, or is thinnest, at the particular area of the shaft that was shown to fail. The only way to rationalize a neck fracture from the results of this study would be to assume that a neck fracture would occur when a force is subjected to the side of the bone, directly at the neck. This can be assumed because of the results at the 90° orientation, in which the fracture occurred at the location of the applied force. This is not an unreasonable assumption, as the boxer's fracture occurs due to improper punching form, so it is a possibility that the side of the neck is what comes in contact with the hard surface.

In terms of prevention, forces to the lateral side of the bone should be avoided or damped, as the bone will fracture easier than when subjected to a force perpendicular to its longitudinal axis. This again stems from the results at an orientation of 90°. Padding can be added to the side of gloves to damp the force on the side of the hand. This can apply to sports such as baseball/softball and football, in which gloves are commonly used. A common situation would be when a baseball/softball player is at bat, where there is a chance that a poorly thrown pitch could hit the side of the athlete's hand. The same concept applies to non-athletes as well – it is important to protect the lateral side of the hand, rather than just the knuckles.

In terms of overall understanding of the boxer's fracture, this investigation provided useful insight into the general mechanics of the fifth metacarpal. However, to truly assist surgeons in treatment of this injury, further investigation is required. The addition of clinical observations will provide valuable insight that would further validate the results of this study. Furthermore, improvements can be made in the mechanical analysis. For the experimental procedure, the testing of actual bone samples would be ideal, as it would account for the internal geometry and material properties that could in fact cause the bone to fracture in different locations. The FEA model can also be refined to better simulate an actual bone. The inside of the geometry can be modeled similarly to the internal structure of bone, and more material properties can be specified in the model. The fixed supports and forces can also be refined to more accurately represent the anatomic constraints in the hand.

## **6 Conclusions**

In this paper, the biomechanics of the boxer's fracture were analyzed through experimental and analytical methods. The results from both investigations demonstrated that the geometry of the fifth metacarpal bone optimizes the bone for compressive loads. This study also yielded that the boxer's fracture is most likely to occur in the shaft of the bone when loaded axially, and that the bone would fracture at the location of the applied force when the force is applied to the lateral



side of the hand. The paper outlines some suggestions as to how to prevent the injury, but further investigation is required to gain full understanding of the boxer's fracture.

### Acknowledgements

The authors acknowledge Jared Schatzinger at the Ohio Northern University for his help and support with the 3D scanner and 3D printer. The authors also acknowledge the financial support of the National Science Foundation through grant number DMR-0423914.

### Appendix

Figure A.1: Images of experimental test samples at orientations of  $0^\circ$  (Left),  $30^\circ$  (Middle), and  $60^\circ$  (Right).

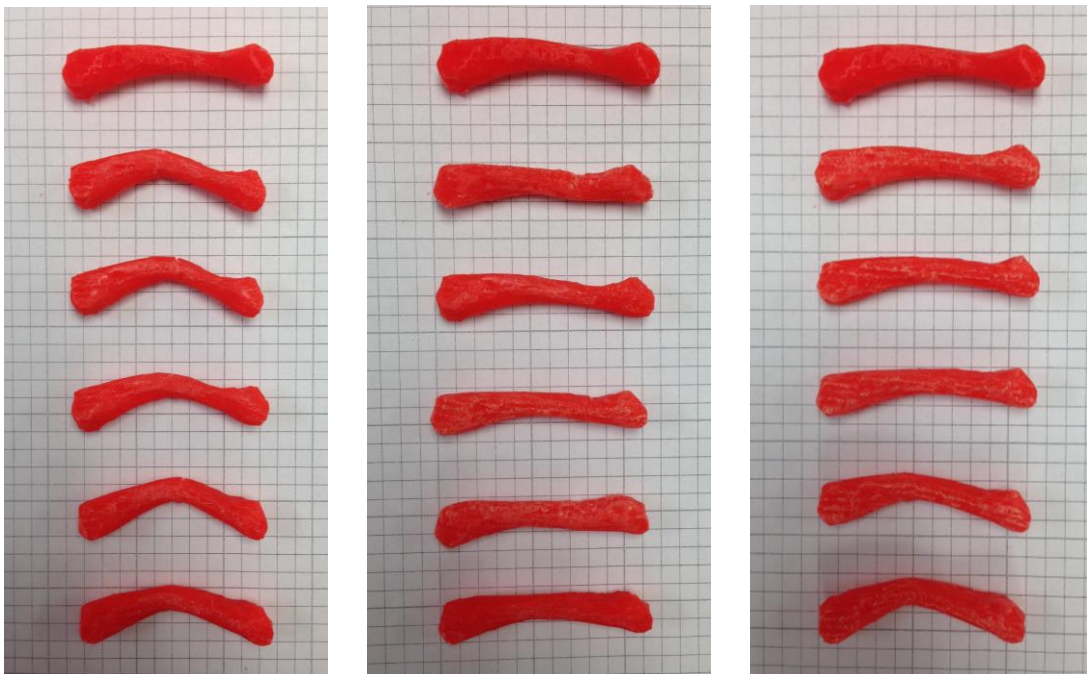
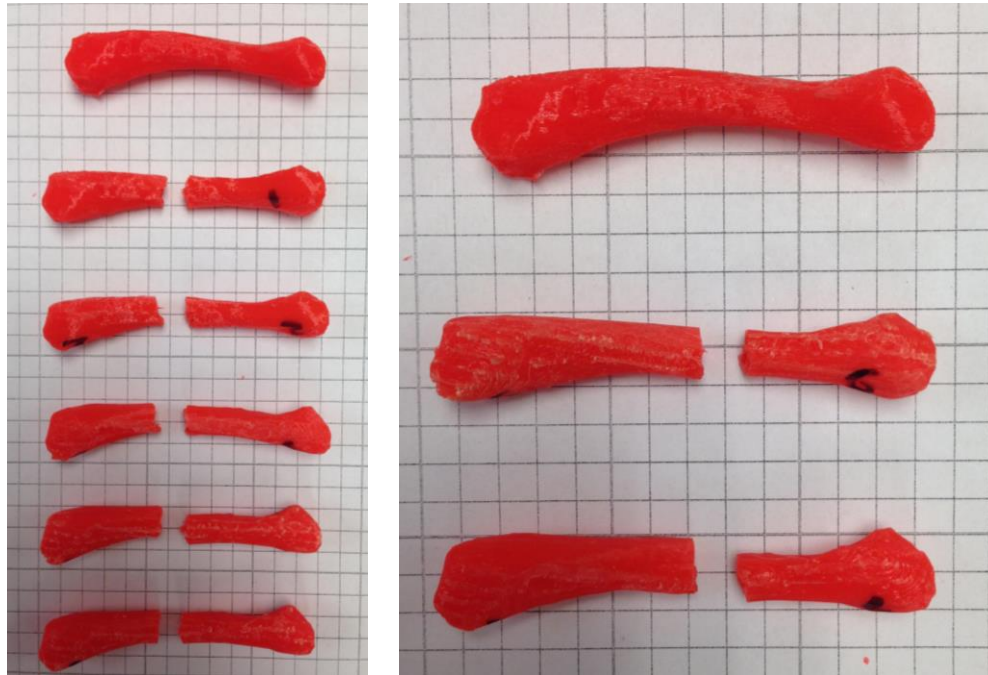


Figure A.2: Images of experimental test samples at 90° orientation with Force 1 (Left) and Force 2 (Right).



## References

- [1] Harris, A. R., Beckenbaugh, R. D., Netteur, J. F., and Rizzo, M., 2009, "Metacarpal Neck Fractures: Results of Treatment with Traction Reduction and Cast Immobilization," *American Association for Hand Surgery*, 4, pp. 161-164.
- [2] Greer, S. E., Williams, J. M., 1999, "Boxer's Fracture: An Indicator of Intentional and Recurrent Injury," *American Journal of Emergency Medicine*, 17(4), pp. 357-360.
- [3] Muller, M. G. S., Poolman, R. W., van Hoogstraten, M. J., Steller, E. P., 2003, "Immediate mobilization gives good results in boxer's fractures with volar angulation up to 70 degrees: a prospective randomized trial comparing immediate mobilization with cast immobilization," *Arch Orthop Trauma Surg*, 123, pp. 534-537.
- [4] Potenza, V., Caterini, R., De Maio, F., Bisicchia, S., Farsetti, P., 2012, "Fractures of the neck of the fifth metacarpal bone. Medium-term results in 28 cases treated by percutaneous transverse pinning," *Injury, Int. J. Care Injured*, 43, pp. 242-245.
- [5] Ali, A., Hamman, J., Mass, D. P., 1999, "The Biomechanical Effects of Angulated Boxer's Fractures," *Journal of Hand Surgery*, 24(A), pp. 835-844.
- [6] Soong, M., Got, C., Katarincic, J., 2010, "Ring and Little Finger Metacarpal Fractures: Mechanisms, Locations, and Radiographic Parameters," *Journal of Hand Surgery*, 35(A), pp. 1256-1259.
- [7] Ethier, C. R., Simmons, C. A., 2007, *Introductory Biomechanics: From Cells to Organisms*, Cambridge University Press, Cambridge, pp. 379-397, Chap. 9.